The electronic structure of liquid and amorphous Se: chain models

1997 J. Phys.: Condens. Matter 9 613

(http://iopscience.iop.org/0953-8984/9/3/003)

J. Phys.: Condens. Matter **9** (1997) 613–626. Printed in the UK PII: S0953-8984(97)74479-5

The electronic structure of liquid and amorphous Se: chain models

Thorsten Koslowski

Institut für Physikalische Chemie und Elektrochemie I, Universität Karlsruhe, Kaiserstraße 12, D-76128 Karlsruhe, Germany

Received 14 May 1996

Abstract. We present a numerical study of the electronic structure of simple models of liquid and amorphous selenium. The geometry is based upon random walks; the electronic structure is described by a tight-binding Hamiltonian. We investigate the influence of the bond- and dihedral-angle distribution, the range and nature of the tight-binding hopping matrix element and the sign and magnitude of the electron–electron interaction upon the density of states. Localization properties and charge profiles have been computed.

To reproduce the experimentally observed optical gap, it is essential to fix the dihedral angles and to introduce an intraorbital electron–electron attraction of modest strength ($U \simeq -2$ eV). In contrast to local descriptions of bond breaking in disordered Se, we observe the formation of two negatively charged chain ends, compensated by the creation of a bipolaron within the chain. Only bipolaron states are able to occupy an impurity band. A simple mechanism for Fermi level pinning is discussed. We give an outlook on the electronic properties of related three-dimensional models.

1. Introduction

The unique and striking properties of liquid and amorphous selenium have provoked a vast amount of experimental and theoretical studies on the geometry and the electronic structure of this element in its disordered state [1–3]. At the melting point, the highly viscous liquid Se is believed to consist of chains of $n = 10^5$ to 10^6 atoms [4]. The structure of Se under these conditions can be described by a random-chain model [5, 6], with nearest-neighbour distances and bond angles similar to those of the crystalline solid ($r_0 = 2.373$ Å, bond angle $\phi = 103.1^\circ$ and dihedral angle $\psi = 100.6^\circ$ [7]). The existence of a ring-chain equilibrium for liquid Se has been challenged [8], whereas a ^{77}Se NMR study by Warren and Dupree [9] has confirmed the shortening of Se chains with increasing temperature. As the radial distribution functions for liquid and amorphous Se show the same basic features—as indicated by neutron scattering experiments [10, 11]—and as we are interested in the electronic structure and less so in dynamical properties, we will in the following treat the two types of disorder on an equal footing.

Only quite recently has liquid Se attracted the attention of computational chemists and physicists. Balasubramanian *et al* [12] have simulated ensembles of short Se chains using a harmonic potential between nearest neighbours and the Lennard-Jones potential for all other interatomic interactions. Bichara and co-workers [13] have performed a tight-binding Monte Carlo simulation of liquid Se, using a short-range soft-sphere repulsion and a moment approximation to the local tight-binding density of states. The authors find a completely

0953-8984/97/030613+14$19.50

different local arrangement of selenium atoms to that in the simple chain model: Se chains are comparatively short, and a large number of threefold-coordinated Se atoms compensates the number of chain ends, leading to an average coordination number of two. Recently, attempts to simulate liquid Se utilizing Car–Parrinello molecular dynamics—using the local density approximation (LDA) for the electronic structure calculation—have been performed for small systems [14, 15]. All simulation work cited above leads to—according to the corresponding authors—an excellent agreement of the computed and the experimental pair distribution function. The bond-angle distributions are broad and peak at $\sim 105^{\circ}$. It is one of the aims of this work to address the question of whether the differences in local geometries—manifest in the system's bond or dihedral angles—have a profound influence on the electronic structure and may favour one of the models. For all simulations of Se—classical or quantum mechanical—close to the melting point, the high viscosity of the liquid remains a major challenge. Extremely long MD runs or Monte Carlo techniques of the 'reptation' type [16] are required to explore the configuration space of the polymer properly [17].

Selenium shows semiconducting behaviour in the trigonal crystalline phase (σ from 10^{-5}–10^{-6} S cm^{-1} [18] down to $\sim 10^{-10}$ S cm^{-1} [19], $T = 298$ K), the amorphous phase ($\sigma = 10^{-16}$ S cm^{-1}, $T = 298$ K [20]) and at the melting point ($\sigma = 4 \times 10^{-9}$ S cm^{-1}, $T = 490$ K [19]). Approaching the critical point ($p_c = 380$ bar, $T_c = 1860$ K [21]), strongly enhanced conductivities close to values typical of dirty metallic behaviour (100–300 S cm^{-1}) have been observed. Warren and Dupree have suggested that chain shortening may be responsible for the conductivity enhancement [9], an interpretation supported by a recent study of the localization properties of a lattice model of liquid Se [22]. Despite the highly disordered nature of the amorphous solid, Se atoms do not carry local magnetic moments as deduced from the absence of a corresponding ESR signal [23], whereas in the liquid phase there is clear evidence for paramagnetism above 1073 K [24]. The paramagnetic contribution to the susceptibility of the liquid has an activation energy of 0.66 eV over most of the semiconducting transport regime.

The electronic structure of disordered Se has been discussed by Street, Mott and Davis (see [25]) and by Kastner, Adler and Fritzsche (KAF) [26] within a picture of local chemical bonding. Supported by Anderson's hypothesis of an effective electron–electron attraction in systems with a strong degree of electron–phonon coupling [27], Street and Mott have argued that a Se–Se bond is likely to be broken heterolytically [25]. The reaction $2D^0 \rightarrow D^+ + D^-$ is favoured by a change of the internal energy of the order of the strength of the electron–electron attraction, U (the underlying Hubbard model will be described below). In the KAF model, a defect and those orbitals on its neighbours that participate in a chemical bond with the defect are considered. The interaction between a singly coordinated, positively charged C_1^+ (D^+) centre and a C_2^0 atom within the chain is considered to be strong enough to lead to the formation of a Se atom with threefold coordination, a C_3^+ centre. As both models are based upon a local picture, they necessarily underestimate the kinetic energy of an electron moving along a Se chain. The influence of the kinetic energy will inevitably broaden the atomic or molecular orbitals into bands and screen the electron–electron interaction, irrespective of its sign.

In this article, we present a simple model of the electronic structure of amorphous and liquid Se. The underlying geometry is based upon random-walk models, and the electronic structure is described by a tight-binding model incorporating the influence of electron–electron interaction. In the following section, details of the model will be presented. For a variety of parameters, the density of states, the localization properties of eigenfunctions and the charge distribution are computed numerically. In the third section, the results thus

obtained are compared to experiments and discussed in the framework of the defect models referred to above. Conclusions are derived in the last section.

2. The model

Bellissent and Tourand [5] have described the geometry of selenium melts up to 1173 K by a model of *nearly free rotating chains (NFRC)*, embedding a coordination number of two, a fixed bond length and a fixed bond angle. The nearest-neighbour peak is given by the bond length, r_0, the position of the next-nearest-neighbour peak is given by $r_1 = 2r_0 \sin(\phi/2)$. Broadening of the first two peaks in the pair distribution function can be modelled by broadening the—still narrow—distributions of bond lengths and bond angles. The computed and experimental structure factors presented by these authors are in excellent agreement. Providing a geometry not in disagreement with experiments, the NFRC model and related concepts are used as highly simplified, but controllable models that form a reasonable basis for electronic structure computations here. The results of these calculations are the key issue of this work.

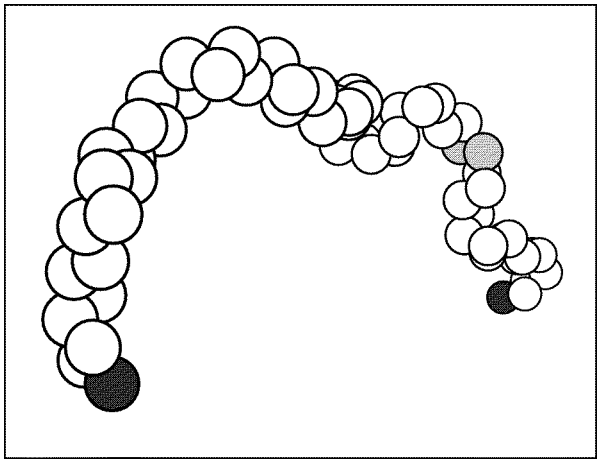

Figure 1. Continuous random walks containing 64 atoms. Charges are indicated by shading. Black: $z \simeq -1$ (C_1^- centres); grey: $z \simeq +1$ (bipolaron); white: $z \simeq 0$.

The geometry of Se is described by random walks of length n, either continuous—identical to the NFRC model once bond angles are fixed—or, with further restrictions—based upon a lattice. A chain on a *lattice random walk (LRW)* is created the following way. The first atom is placed at random on a simple cubic lattice. For the second atom of the chain one of the six nearest-neighbour positions is chosen at random. Further atoms are added in one of the four nearest-neighbour positions of the head atom that give rise to a bond angle of $\pi/2$ until the desired number of atoms n per chain is met. For a *continuous random walk (CRW)*, new atoms are created at random on a sphere of radius r_0—the average liquid nearest-neighbour distance of 2.38 Å—around the head atom. Using a rejection technique [28], additional constraints like the limitation of the bond angle to $\pi/2$ can be introduced. The CRW dihedral-angle distributions are continuous, whereas the LRW dihedral angle can only take the values of zero, $\pi/2$ and π. For a fixed chain length n, the geometry of the models presented here can be classified as either based upon a LRW or a CRW; in the latter case the bond angle is either random ($p(\phi) \propto \sin\phi$) or takes the value of $\pi/2$. An example

of a continuous random walk is presented in figure 1. Naturally, random walks can be folded into a simulation box of length $L = (n/\rho)^{1/3}$ with periodic boundary conditions.

The electronic structure of the model is described by a tight-binding Hamiltonian using a basis set of three 4p orbitals centred on each selenium atom:

$$H = \sum_{a\neq b=1}^{n} \sum_{i,j=1}^{3} c_{ia}^{\dagger} c_{jb} V_{iajb}. \tag{2.1}$$

As in all simplified treatments of Se, the low-lying 4s orbital is ignored. The $c_{ia}^{\dagger}/c_{ia}$ are creation/annihilation operators acting upon atomic orbitals $|ia\rangle$ localized at Se atoms with index a. The hopping matrix elements are assumed to depend on the interatomic distance following Bichara *et al* [13]:

$$V_{iajb}(r_{ab}) = V_0 \exp(-q r_{ab}) \tag{2.2}$$

with $q = 1.628$ Å^{-1}, $V_0^{pp\sigma} = 133$ eV for σ bonds and $V_0^{pp\pi} = -35$ eV for π bonds, leading to $V_{pp\sigma}(r_0) = 2.95$ eV and $V_{pp\sigma}(r_0) = -0.78$ eV. The zero of the energy scale is arbitrary. For any arrangement of Se atoms not based upon a cubic lattice with nearest-neighbour interactions only, σ and π contributions have to be weighted according to the Slater–Koster rules [29]. Modelling liquid Se by a random walk naturally neglects some of the three-dimensional aspects of the electronic structure. The second peak in the radial distribution function (at $r \sim 4$ Å) is usually interpreted as stemming from two topological next-nearest neighbours and a shell of Se atoms residing either on different chains or on the same chain, more than two chemical bonds away. Topological next-nearest neighbours are considered in some of the model Hamiltonians described below; other tight-binding interactions will slightly broaden the density of states and may require a minor reparametrization. The situation changes significantly once threefold-coordinated Se atoms are introduced. Some aspects of these C_3 centres will be discussed below, whereas a detailed numerical study of their influence on the electronic structure will be the subject of future work.

Electron correlation is considered via the familiar Hubbard model [30] of intraorbital electron–electron interaction. The thus-extended tight-binding Hamiltonian (2.1) now reads

$$H = \sum_{a\neq b,i,j,\sigma} c_{ia\sigma}^{\dagger} c_{jb\sigma} V_{iajb} + \frac{U}{2} \sum_{ai\sigma} n_{ai\sigma} n_{ai-\sigma} \tag{2.3}$$

with the number operator $n_{ai\sigma} = c_{ai}^{\dagger} c_{ai}$. The disordered Hubbard Hamiltonian can be solved self-consistently using the unrestricted Hartree–Fock (UHF) approximation $n_{ai\sigma} n_{ai-\sigma} \simeq n_{ai\sigma}\langle n_{ai-\sigma}\rangle + \langle n_{ai\sigma}\rangle n_{ai-\sigma} - \langle n_{ai\sigma}\rangle\langle n_{ai-\sigma}\rangle$ where the brackets indicate the computation of ground-state expectation values, in this case from a previous SCF step. The (Ising spin) UHF problem factorizes into an up-spin Hamiltonian:

$$H_{\sigma}^{UHF} = \sum_{a\neq b,i,j} c_{ia\sigma}^{\dagger} c_{jb\sigma} V_{iajb} + U \sum_{ai} n_{ai\sigma} \langle n_{ai-\sigma}\rangle \tag{2.4}$$

and a similar Hamiltonian for the down spin. Local (orbital) magnetic moments are given by $\mu_{ai} = \langle n_{ai\sigma}\rangle - \langle n_{ai-\sigma}\rangle$, and local charges by $n_{ai} = \langle n_{ai\sigma}\rangle + \langle n_{ai-\sigma}\rangle$. U denotes the effective electron–electron interaction, including a possible reduction by electron–phonon coupling.

As we are interested in the contribution of certain atoms—particularly of the C_1 defects located at the ends of the polymer chain—to the density of states, we perform a population analysis [31]. The charge order q_α of an eigenstate $|\alpha\rangle$ with energy E_α with respect to an atomic orbital $|ai\rangle$ is given by $q_\alpha^{ia} = |\langle\alpha|ai\rangle|^2$. The product of the DOS and q_α^{ai} equals the partial density of states (PDOS).

Table 1. Chain models of Se discussed in this work. Z_{TB} denotes twice the range of the tight-binding interaction, σ and π denote the type of the chemical bond, U the strength of the electron–electron interaction, LRW stands for a lattice random walk, and CRW for a continuous random walk.

Index	σ	π	Z_{TB}	Bond angle	Random walk	U (eV)	DOS figure
1	+	+	2	$\pi/2$	LRW	0	2(a)
2	+	+	4	$\pi/2$	LRW	0	2(b)
3	−	+	4	$\pi/2$	LRW	0	—
4	+	−	4	$\pi/2$	LRW	0	—
5	+	+	2	$\pi/2$	CRW	0	—
6	+	+	2	Random	CRW	0	—
7	+	+	4	$\pi/2$	CRW	0	—
8	+	+	4	Random	CRW	0	2(c)
9	+	−	4	$\pi/2$	CRW	0	—
10	+	−	4	Random	CRW	0	—
11	+	+	4	$\geqslant \pi/2$	CRW	0	—
12	+	+	2	$\geqslant \pi/2$	CRW	0	—
13	+	+	4	$\pi/2$	LRW	−2	3(b)
14	+	+	4	$\pi/2$	LRW	+2	3(a)
15	+	+	4	$\pi/2$	CRW	−2	3(c)
16	+	+	4	$\pi/2$	CRW	+2	—

Assuming that the expansion coefficients $a_{ia}^{\alpha} = \langle \alpha | ai \rangle$ of a wave function of a disordered one-dimensional system show an exponential decay [32] of the type

$$|a_{bi}^{\alpha}| = |a_{0i}^{\alpha}| \exp(-\gamma_{\alpha} b) \tag{2.5}$$

the localization length $L_{loc} = 1/\gamma$ (for clarity, the index α will be skipped) can be computed from

$$\gamma = -\frac{1}{b} \lim_{b \to \infty} \ln |a_{bi}|. \tag{2.6}$$

In the theory of discrete maps, γ is called the Lyapunov exponent. For Se chains occupying a cubic lattice with nearest-neighbour interactions—such as the models 1–4, 13 and 14 referred to in table 1—the Hamiltonians (2.2) and (2.4) can be separated into p_x, p_y and p_z problems with a one-dimensional topology. The wave-function expansion coefficients can be generated recursively:

$$a_{b+1} = \frac{1}{V_{b,b+1}} [(E - \epsilon_b) a_b + V_{b,b-1} a_{b-1}] \tag{2.7}$$

with appropriate starting coefficients $a_{-1} = 0$ and $a_0 = -V_{12}$. As we deal with only one orbital per site, the index i has been skipped. To avoid numerical overflow when applying (2.7), the current coefficients have to be renormalized and the normalization constants are accumulated to compute γ [33].

3. Results and discussion

The influence of the following quantities and parameters—defining the geometry and the Hamiltonian of the simple chain model—upon the density of states has been studied systematically.

(1) The bond angle (either obeying a value of $\pi/2$ or following a random distribution).
(2) The dihedral-angle distribution via the type of the random walk.
(3) The nature of the tight-binding hopping matrix element (σ, π or σ and π combined).
(4) The coordination number Z_{TB}—defined as the number of neighbours to which hopping is enabled by a non-zero matrix element (2.2).
(5) The strength and sign of the electron–electron interaction parameter, U.

For a complete list of models see table 1. For each model 1000 realizations for chains of length $n = 64$ have been accumulated. Whenever the rôle of defects is of interest, the use of short chains leads to a high statistical efficiency. As will be discussed below, the length scale relevant for electronic properties is much smaller than n.

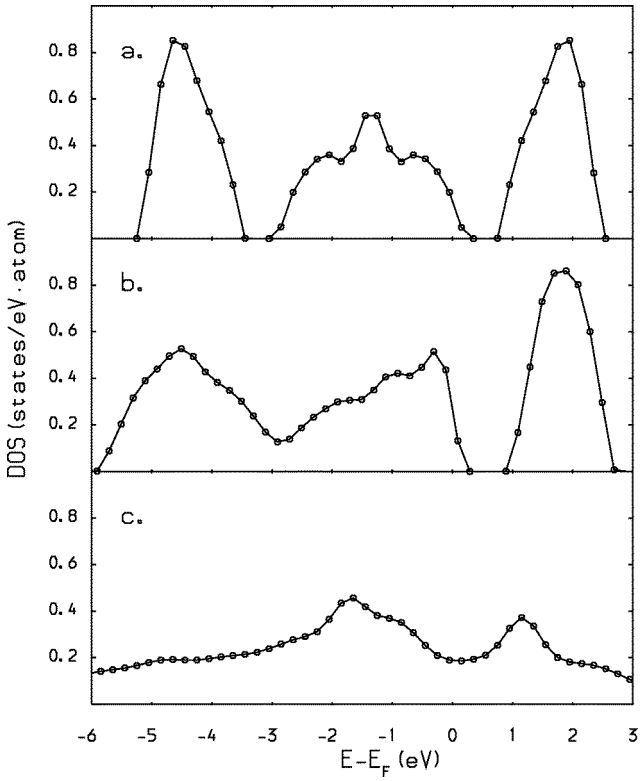

Figure 2. Densities of states for models 1 (a), 2 (b) and 8 (c); see table 1 and the text for details. The energies are in electron volts; the densities of states are given per electron volt and atom.

With the help of figure 2(a) (model 1, the index refers to table 1) we illustrate the general form of the density of states obtained for the models of Se presented here. Starting from the lowest energies, a bonding σ band is separated from a π band that is split into a lower bonding and an upper antibonding band. The spike at $E = 0$ eV is caused by C_1 defect states, i.e. non-bonding orbitals not participating in bonds at the chain ends. This has been confirmed by a population analysis, indicating a defect charge order $q(E = 0) \simeq 0.16$ in fourfold excess of the average value of 1/32. In the absence of diagonal disorder, a chain with nearest-neighbour hopping represents a bipartite system with a symmetric spectrum around $E = 0$. So an antibonding σ^* band is separated from the π band by a small band

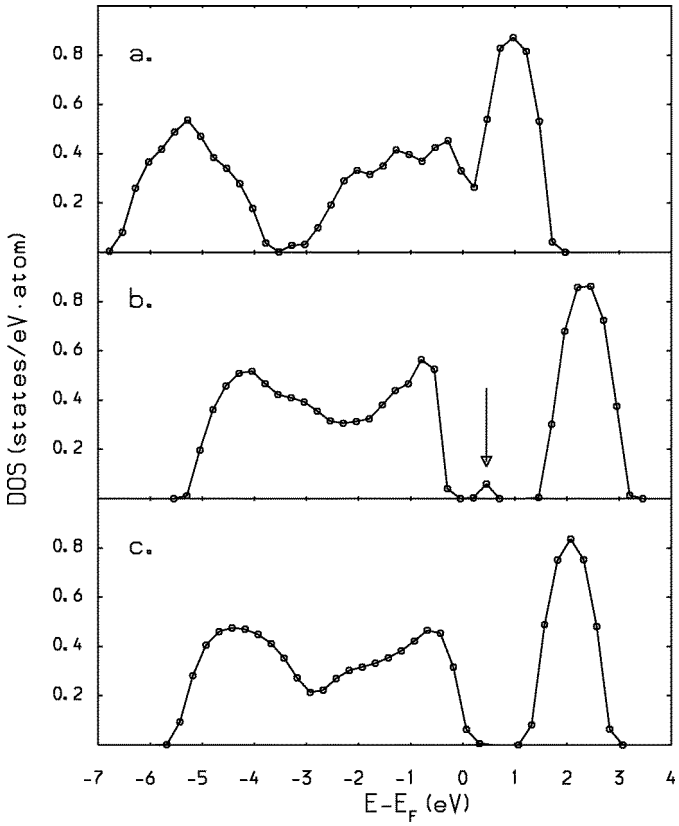

Figure 3. Densities of states for models 14 (a), 13 (b) and 15 (c); see table 1 and the text for details. The energies are in electron volts; the densities of states are given per electron volt and atom.

gap. For a finite chain, the Fermi level is trivially pinned at the upper band edge of the π band, and adding or removing an electron does not affect the position of E_F drastically. Only for an infinite or cyclic chain is the Fermi level located between the π and the σ^* band.

Once next-nearest-neighbour interactions are considered (model 2, figure 2(b)) the particle–hole symmetry is broken, and the σ and π bands overlap, whereas the shape and the position of the σ^* band are essentially conserved. Vestiges of the former π/π^* band are manifest as shoulders at around $E = 0$. A rough identification of σ and π bands in the absence of separability is provided by setting either the σ or the π interaction to zero.

The density of states exhibits only minor changes if the LRW geometry is replaced by a continuous random walk, provided that the bond angle is fixed at $\pi/2$. This behaviour is independent of the range of the hopping matrix elements (model 1 $\rightarrow$ model 5, model 2 $\rightarrow$ model 7). However, once the bond angle is randomized, all bands are not only broadened, but become essentially structureless. The Fermi level is located in a local minimum of the density of states, with a large DOS(E_F). A typical example is presented in figure 2(c) (model 8). This behaviour again does not depend on Z_{TB} and is observed even in the absence of π interactions. Restricting the random bond angle to values larger than $\pi/2$ does not alter the DOS significantly (models 11 and 12).

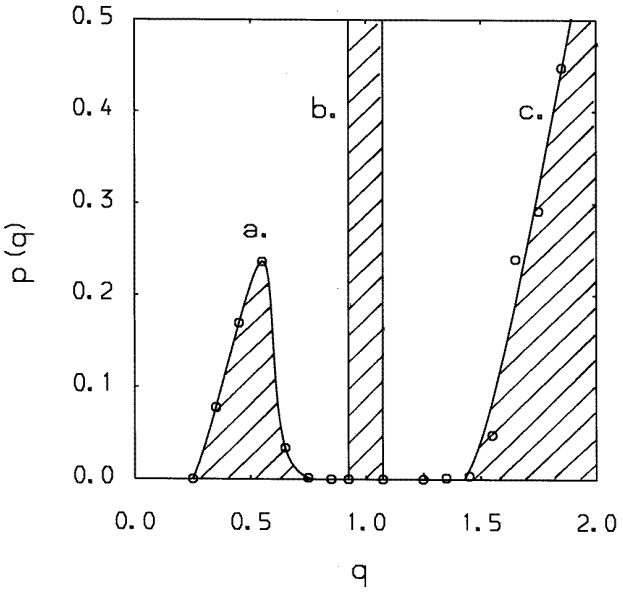

Figure 4. The orbital electronic population probability distribution $p(q)$ for model 13; see table 1 for details. The electronic charges are in units of e.

Electron–electron interaction plays a dominant rôle in low-dimensional systems. We consider both electron–electron repulsion and attraction of a moderate strength of $U = \pm 2$ eV. Starting from model 2 ($Z_{TB} = 4$, σ and π interactions, LRW geometry), a repulsive Hubbard U changes the relative positions of the band centres as follows: the π band is shifted to higher energies, reducing the gap between the valence band and the σ^* conduction band. The relative position of the σ band with respect to the centre of the σ^* band is almost unchanged (figure 3(a)). Like for transition metal and rare-earth compounds, a small band width—tantamount to a low kinetic energy as typical for π compared to σ bands—does inevitably enhance the influence of electron–electron interaction. A negative Hubbard U has the opposite influence: the centre of the π band is shifted towards lower energies—taking the centre of the unoccupied σ^* band as a reference energy—and shows a stronger overlap with the σ band (figure 3(b)). At the top of the valence band, a small impurity band—indicated by an arrow in figure 3(b)—is split from the bulk of the density of states. The Fermi level is now pinned in a small gap between the impurity band and the bulk DOS. Although the number of states in the impurity band equals the number of chain ends—a fact also confirmed for chains of different length—their defect charge order is vanishingly small. Within the model described here, the impurity band can thus not be interpreted as a band originating from C_1 centres.

From the energy-resolved defect charge order it rather transpires that states located at E_F in the absence of electron–electron interactions are now shifted into the interior of the valence band by roughly 2 eV. Both ends of the chains carry an excess charge of one electron, transforming them into C_1^- centres. The excess positive charge is moved into the interior of the chain; its localization characteristics will be discussed below. It is interesting to note that Warren and Dupree [9] have postulated a density of states similar in appearance to figure 3(b) for Se close to the melting point. We have, however, to indicate again that according to our model calculations the states in the impurity band do *not* originate from

C_1 states, as assumed by these authors. Replacing the LRW by a CRW geometry, we notice that the gap between the valence band and the impurity band has vanished (figure 3(c)) and E_F is located in the tail of the valence band again. U has to be decreased to -4 eV to lead to the formation of a C_1^+ and a C_1^- centre. The resulting band gap, however, will be $\sim$1 eV too large compared to experiments and will only partly be compensated by band broadening due to interchain interactions.

As the position of the π valence band relative to the σ^* conduction band is strongly affected by electron–electron interactions, it is the strength of U that controls the size of the band gap. Considering a LRW geometry with σ and π hopping matrix elements extending to next-nearest neighbours, a band gap of 1.1 eV is observed in the absence of electron correlation (model 2); the gap ceases to exist for $U = 2$ eV (model 14); its size is increased to 2.2 eV for $U = -2$ eV (LRW, model 13). The band gap between the bulk of the valence band and the conduction band induced by an on-site electron–electron interaction of $U = -2$ eV is close to the experimentally observed optical gap of $\sim$2 eV [34]. As expected for an intrinsic semiconductor, this is twice the value of the thermal activation energy of the conductivity. We would like to note that despite the large value of U, its contribution to energies of excitation processes may actually be quite small, as spin pairing in a singly occupied orbital can be broken by an energy of $-Un_\uparrow n_\downarrow = 2 \times 1/2 \times 1/2 = 1/2$ eV, further reduced by screening to $(1/2)L_{loc}$ of its initial value, with $L_{loc} \simeq 2$ (see below) denoting the minimum range over which a wave function is spread [35]. For the simple model presented here, we have resisted the temptation of tuning U to meet the experimental value of the band gap and the activation energy. It is interesting to note that in the absence of electron correlation, a band gap consistent with experimental observations can only be obtained by introducing different site energies for σ and π atomic orbitals [36]. We believe that the resulting improvement of the fit of tight-binding band structures to more elaborate schemes or to experiments can be the only motivation for this parametrization. The physical explanation for the observed effect, however, rests in the influence of an effective electron–electron attraction.

The electron population along the chain roughly follows the pattern $q(\mathrm{p}_i) - q(\mathrm{p}_j) - q(\mathrm{p}_k) = (2 - 1 - 1)$ (i, j, k denoting any permutation of x, y, z), and the electron pair does randomly localize on one of the three p orbitals. A total population of four electrons per atom emerges, with the exception of the formation of charged C_1^- centres and the compensation of the defect charge within the chain. None of the models studied here exhibits the formation of local moments, and all spins are paired, as required by the absence of an ESR signal in amorphous Se as referred to above [23]. In a local spin-density/molecular dynamics study of small Se clusters, Hohl and co-workers have noted that the moment-carrying triplet state of linear Se_4 lies $\sim$0.3 eV above the singlet state [37]. Activated paramagnetism in the liquid—as observed by Freyland and Cutler [24]—may find its explanation by a bond-breaking process with a consecutively activated formation of a triplet state—or an otherwise moment-carrying state—from a bipolaronic species.

The probability density $p(q)$ of the orbital charge is plotted in figure 4 [38]. The central peak of $p(q)$ (b) can easily be assigned to a charge of $\sim e$, characteristic for $2(n-2)$ orbitals within the chain and one orbital at each end of the chain, confirmed by an integrated $p(q)$ of 126. The integral over the first peak (a) equals 1, and the last peak (c) has an integrated $p(q)$ of 65, all accurate within the computational round-off error. At each end of the chain, we find two pairs of spin-paired electrons. The excess negative charge is compensated within the chain by reducing the charge of a pair of electrons located at two neighbouring atoms in a twofold way. On the first orbital contributing to the defect, the charge is reduced to an average of $\sim e/2$ (corresponding to peak a), while on an orbital located on a neighbouring

atom, the charge is reduced considerably less to an average of $\sim 1.75e$. The resulting object may be identified as a *bipolaron*. Within the KAF terminology, it can be assigned the symbol $(C_2)_2^{2+}$. This picture has also been confirmed by inspecting the charge distribution of a large number of chains. The discrepancy of the chain end and the compensating charge is due to a charge of singly occupied orbitals slightly less then e and charges of doubly occupied orbitals with charges slightly below $2e$. Since any positively charged defect can be interpreted as an energy barrier for a system characterized by electron–electron attraction, defect pairing reduces the scattering of conduction electrons. It thus enhances the kinetic energy and consequently the band width and the cohesive energy. Whenever the restrictions on the value of the dihedral angles are loosened, the resulting charge distribution is broadened considerably. The resulting charge distribution along the chain is presented in figure 1 for a single realization. It demonstrates that C_1^- centres and bipolarons continue to exist.

It is not unlikely that two C_1^- centres and a bipolaron may react to form a centre with a threefold or fourfold coordination, probably going hand in hand with a redistribution of the bipolaron charge, resulting in similar local geometries to those postulated by KAF. Bipolarons may be considered as structural elements in compounds like $[P(C_6H_5)_4]_2$ $[Se(Se_5)_2]$ (**a**) [39] or $[(C_6H_5)_3PNP(C_6H_5)_3]_2[Se_{10}]\cdot(CH_3)_2N$–CHO (**b**) [40]. The bipolaron is able to attract two C_1^- centres by either the atom carrying the majority positive charge—leading to the formation of compound (**a**)—or by forming bonds between each of the bipolaron Se atoms and a chain end—forming compound (**b**). The excess—formal—negative charge may reside in a non-bonding orbital.

In the following, we will discuss an additional mechanism—arising from the net Coulombic attraction between a bipolaron and two negatively charged chain ends—that may stabilize this peculiar defect configuration. Two strategies will be used to estimate the change of energy induced by two excess electrons localized on the chain ends of a Se polymer and a bipolaron located in the centre of the chain. In the first approach, we ignore the influence of charge ordering upon the polymer geometry and represent the polymer chain by a random walk of length $n = 64$ (i.e. orders of magnitude smaller than the actual chain length) and an end-to-end distance of $\sqrt{n}r_0$. For convenience, the bipolaron charge is considered as being localized on a single Se atom. Using $Z_+ = 2$, $Z_- = -1$ and $\epsilon = 6$ we obtain

$$\Delta U = \frac{e^2}{4\pi\epsilon\epsilon_0 r_0}\left(2\frac{Z_+Z_-}{\sqrt{32}} + \frac{Z_-^2}{\sqrt{64}}\right) \simeq -0.60 \text{ eV}. \tag{3.1}$$

In the second approach, we follow just the opposite strategy: the influence of the polymer geometry is neglected, and only charge ordering via the mean-spherical approximation [41]—or its limiting case, the Debye–Hückel theory of electrolytes—is considered. Using $\rho = 0.025$ atoms Å^{-3} and $k_BT = 0.05$ eV, an inverse Debye–Hückel screening length

$$\kappa_0 = \sqrt{\frac{e^2}{\epsilon\epsilon_0 k_B T}\frac{\rho}{n}(Z_+^2 + 2Z_-^2)} \simeq 1.17 \text{ Å}^{-1} \tag{3.2}$$

leads to an MSA inverse screening length of

$$\Gamma_0 = \frac{-1 + \sqrt{1 + 2\kappa_0 r_0}}{2r_0} \simeq 0.20 \text{ Å}^{-1} \tag{3.3}$$

and a stabilization energy of

$$\Delta U = -\frac{e^2}{4\pi\epsilon\epsilon_0}\frac{\Gamma_0}{1 + \Gamma_0 r_0}(Z_+^2 + 2Z_-^2) \simeq -1.96 \text{ eV} \tag{3.4}$$

per chain. In the limit of large n, both estimates scale like $n^{-1/2}$, so the resulting energy scale becomes less relevant for realistic chain lengths of $\sim 10^5$ close to the melting point.

As stated above, the pair distribution of amorphous Se [10] does not differ significantly from those of the liquid state at the melting point [11]. The short-range order—characterized by the nearest-neighbour bond length and a coordination number of roughly two—persists up to high pressures and temperatures. With increasing temperature, however, the viscosity decreases and the activated paramagnetic susceptibility increases. This gives indirect evidence for the scenario of chain shortening, accompanied by an increasing number of defects. This structural change will basically alter the ratio of the number of bulk states to that of defect states. Chain shortening alone—discussed within a simple one-electron model [22]—moves the Fermi level into the interior of the valence band, until it crosses a mobility edge.

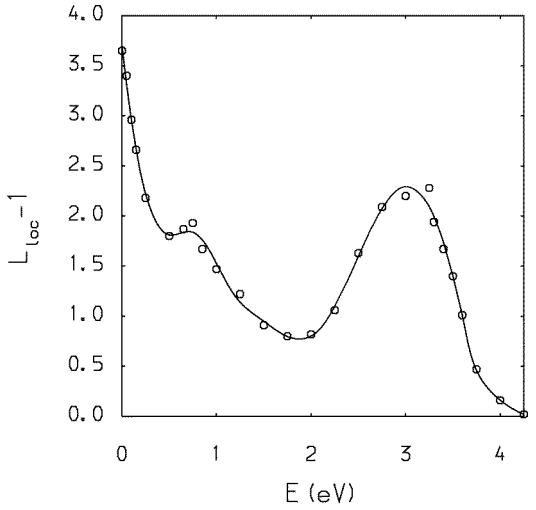

Figure 5. The localization length as a function of energy for a lattice random walk, $Z_{TB} = 4$, σ and π interactions and zero Hubbard U. The localization length is in Se–Se bond lengths; the energy is in electron volts. $E_F = 1.21$ eV.

As described above, for a one-dimensional system with nearest-neighbour interactions only, the localization length L_{loc} can be computed iteratively. L_{loc} as a function of energy is plotted in figure 5. We use a topological unit of length, L_{loc} being given by the number of Se–Se bonds over which the wave function is spread. Obviously, L_{loc} has to be larger than or equal to one. A geometrical—one-dimensional—localization length can be obtained by multiplying L_{loc} by the Se–Se bond length, and any three-dimensional measure of localization would have to embody the *local* centre-of-mass configuration of the random walk (note that the proportionality of the end-to-end distance to $\sqrt{n}$ is valid only in the limit of large distances). Like in any system dominated by off-diagonal disorder, the localization length exhibits a singularity at $E = 0$. This singularity has been damped by introducing a small amount of diagonal disorder obeying a box distribution in the interval $[-0.1\ \text{eV}, 0.1\ \text{eV}]$. With increasing energy, the localization length is influenced by two trends: it reflects both the density of states—the smaller the DOS, the smaller L_{loc}—and exhibits a general decay towards higher energies. A local minimum of the localization length naturally lies between the π band and the σ^* conduction band in a region of an exponentially small density of states. The limiting value of one is reached at the top of the

conduction band. As L_{loc} never exceeds a value of five, all electronic phenomena in the one-dimensional model of Se presented here are governed by this length scale. Thus the choice of a chain length $n = 64 > L_{loc}$ can be justified *a posteriori*. We have performed $b_{max} = 10^6$ iterations of scheme (2.7), with a relative accuracy of $\epsilon = \sqrt{L_{loc}/b_{max}} \leqslant 2.3 \times 10^{-3}$ [42].

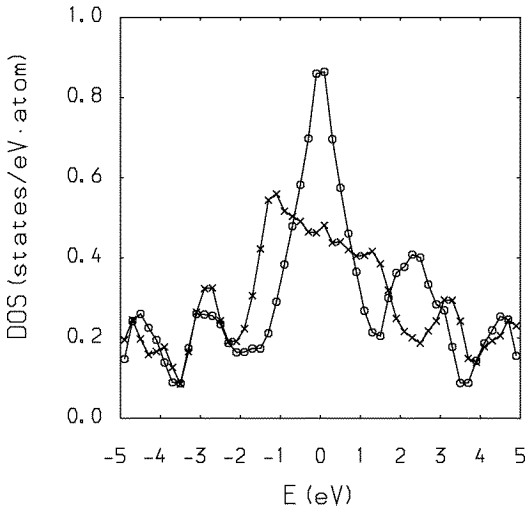

Figure 6. The density of states based upon geometries created by a classical Monte Carlo simulation with chains of length 64 (○, $E_F = 1.08$ eV) and tight-binding Monte Carlo simulations (×, $E_F = 2.33$ eV). The energy is in electron volts; the density of states is given per electron volt and atom.

In the following, we will discuss preliminary results of the electronic structure obtained from three-dimensional geometries and compare them to the chain models described above. As the molecular dynamics [12], tight-binding Monte Carlo [13] and Car–Parrinello MD simulations [14, 15] cited above show a broad distribution of bond angles—and consequently randomized dihedral angles—it is no surprise that their density of states shows features similar to the CRW models with a random bond angle described in this work. We have simulated systems containing eight chains of 64 atoms close to the melting point using the potential of Balasubramanian and co-workers [12]. In addition, small tight-binding Monte Carlo simulations of systems containing 64 atoms have been performed. The coordination number and the position of the first two peaks of the pair distribution functions are in good agreement with the data reported by the corresponding authors. Computing the tight-binding density of states using the Hamiltonian (2.1), we observe a broad, but structured band that does not exhibit a band gap—or even a particularly small density of states at the Fermi level—in either case (cf. figure 6). We think that the tight-binding Monte Carlo simulation would greatly benefit from the consideration of electron–electron interaction effects.

4. Conclusions

We have presented a computational study of the electronic structure of simple models of the disordered phases of selenium. The geometry has been modelled by random walks, while the electronic properties have been computed using a tight-binding Hamiltonian. The single-site (or zero-dimensional) models of Kastner, Adler and Fritzsche [26] or Street, Mott and Davis (see [25]) are thus extended by electron hopping along the direction of the

strongest tight-binding matrix elements.

Electron–electron interaction—both repulsive and attractive—has been incorporated using the Hubbard model, and it turns out to be crucial for reproducing the size of the band gap. It provides a simple physical justification of the difference in σ and π on-site energies in previous tight-binding schemes [36].

The subtle interplay between effective electron–electron attraction and disorder leads to the formation of a type of defect that has not been postulated for the disordered phases of Se before: a *bipolaron* formed within the chain compensating two negatively charged chain ends. A bipolaron impurity band is split from the valence band or lies at its upper edge, pinning the Fermi level.

Using an iteration technique, we have been able to compute the localization length as a function of energy. In a model with nearest-neighbour hopping, Fermi level eigenstates are always strongly localized on a length scale less than that of two Se bonds. The computed localization length serves as a lower boundary to the localization length that can be expected on coupling the chain weakly to a three-dimensional system.

Acknowledgments

It is a pleasure to thank W Freyland for his support and his interest in this work and W von Niessen for many helpful comments on the manuscript. Fruitful discussions with U Beck, C Bichara, J M Holender, D Nattland and M Parrinello are gratefully acknowledged. This work was supported by the Deutsche Forschungsgemeinschaft and—in parts—by the Fonds der Chemischen Industrie.

References

[1] Zhigaro R A and Cooper W C (ed) 1974 *Selenium* (New York: Van Nostrand)
[2] Gerlach E and Grosse P (ed) 1979 *Selenium and Tellurium* (Berlin: Springer)
[3] Hensel F 1980 *Angew. Chem.* **92** 598
[4] Keezer R C and Bailey M W 1967 *Mater. Res. Bull.* **2** 158
[5] Bellissent R and Tourand G 1977 *Proc. 7th Conf. on Amorphous and Liquid Semiconductors* ed W E Spear, p 98
after
Bellissent R and Tourand G 1980 *J. Non-Cryst. Solids* **35–36** 1221
[6] Misawa M and Suzuki K 1978 *J. Phys. Soc. Japan* **44** 162
[7] Krebs H 1968 *Grundzüge der Anorganischen Kristallchemie* (Stuttgart: Enke)
after [34].
[8] Lucovsky G 1979 *Selenium and Tellurium* ed E Gerlach and P Grosse (Berlin: Springer)
[9] Warren W W and Dupree R 1980 *Phys. Rev.* B **22** 2257
[10] Kaplow R, Howe T R and Averbach B L 1968 *Phys. Rev.* **168** 1086
[11] Misawa M and Suzuki K 1977 *Trans. Japan Inst. Met.* **18** 427
Edeling M and Freyland W 1981 *Ber. Bunsenges. Phys. Chem.* **85** 1049
[12] Balasubramanian S, Damodaran K V and Rao K J 1992 *Chem. Phys.* **166** 131
[13] Bichara C, Pellegatti A and Gaspard J-P 1994 *Phys. Rev.* B **49** 6581
[14] Hohl D and Jones R 1991 *Phys. Rev.* B **43** 3856; 1990 *J. Non-Cryst. Solids* **117–118** 922
[15] Holender J M 1995 private communication
[16] Wall F T and Mandel F 1975 *J. Chem. Phys.* **63** 4592
de Gennes P 1971 *J. Chem. Phys.* **55** 572
[17] Parrinello M 1995 private communication
[18] Stuke J 1974 *Selenium* ed R A Zhigaro and W C Cooper (New York: Van Nostrand)
[19] Eckhard F 1954 *Ann. Phys., Lpz.* **14** 233
[20] Hartke J L 1962 *Phys. Rev.* **125** 1177
[21] Hensel F 1976 *Ber. Bunsenges. Phys. Chem.* **80** 786

[22] Koslowski T and von Niessen W 1994 *Phys. Rev.* B **49** 11 704
[23] Abkowitz M 1967 *J. Chem. Phys.* **46** 4537
[24] Freyland W and Cutler M 1980 *J. Chem. Soc. Faraday Trans.* II **76** 756
[25] Street R A and Mott N F 1975 *Phys. Rev. Lett.* **35** 1293
Mott N F, Davis E A and Street R A 1975 *Phil. Mag.* **32** 961
[26] Kastner M, Adler D and Fritzsche H 1976 *Phys. Rev. Lett.* **37** 1504
[27] Anderson P W 1975 *Phys. Rev. Lett.* **34** 953
[28] von Neumann J 1951 *US NBS Appl. Math. Ser.* **12** 36
[29] Slater J C and Koster G F 1953 *Phys. Rev.* **94** 1498
[30] Hubbard J 1963 *Proc. R. Soc.* A **276** 238; 1964 *Proc. R. Soc.* A **281** 401
[31] Mulliken R S 1955 *J. Chem. Phys.* **23** 1833
[32] Mott N F and Twose W D 1961 *Adv. Phys.* **10** 107
[33] Dücker H, Struck M, Koslowski T and von Niessen W 1994 *Phys. Rev.* B **46** 13 087
[34] Optical gap and activation energies after
Feltz A 1993 *Amorphous Inorganic Materials and Glasses* 2nd edn (Weinheim: VCH) p 185
[35] Logan D E and Siringo F 1992 *J. Phys.: Condens. Matter* **4** 3695
[36] Robertson J 1983 *Adv. Phys.* **32** 361
[37] Hohl D, Jones R O, Car R and Parrinello M 1987 *Chem. Phys. Lett.* **139** 540
[38] For completeness, we will give the $p(q)$ values outside the range of figure 4: $p(q = 0.975) = 20.23$, $p(q = 1.025) = 42.76$, $p(q = 1.975) = 31.49$.
[39] Krebs B E, Lührs E, Willmer R and Ahlers F-P 1991 *Z. Anorg. Allg. Chem.* **592** 17
[40] Kräuter G, Dehnicke K and Fenske D 1990 *Angew. Chem.* **102** 421
[41] Waisman E and Lebowitz J L 1982 *J. Chem. Phys.* **56** 3086, 3093
Blum L 1975 *Mol. Phys.* **30** 1529
Blum L and Høye S 1977 *J. Phys. Chem.* **81** 1311
[42] Abrahams E and Steven M 1980 *J. Phys. C: Solid State Phys.* **13** L377
Sak J and Kramer B 1981 *Phys. Rev.* B **24** 1716